PEER-REVIEWED **STOCK PREPARATION**

Concentric mixing of hardwood pulp and water

Aklilu T. G. Giorges, David E. White, and Theodore J. Heindel

ABSTRACT

We completed concentric mixing experiments with velocity ratios of up to 6 using hardwood pulp of 1.0%, 1.9%, and 2.9% consistency and water. By increasing the velocity ratio (ratio of inner:outer jet velocity), we found the inner jet spread angle to be larger and the downstream mixing region uniform. Furthermore, local consistency measurements show a flattening of the concentration profile with increasing velocity ratio, confirming mixing improves as velocity ratio increases.

For the fiber stock tested, mixing was significantly dependent on the stock consistency when the velocity ratio is small ($R_v \cong 1$). This result indicates that the fluid streams do not deliver the shear stress and turbulence required to fully dislodge the fiber network. Mixing results from hydrodynamic instabilities and macroscale variations, which lead to downstream nonuniformities.

At higher velocity ratios when the flow is turbulent, mixing is significantly affected by the velocity ratio, but there is no clear indication that mixing is affected by the stock consistency. These trends are evidence that once the fiber network strength is overcome by shear stress and turbulence, the mixture behaves as a conventional Newtonian fluid in turbulent flow. Mixing at high velocity ratio results from microscale turbulence that leads to a relatively uniform downstream mixture.

Application: This study demonstrates the importance of high velocity ratio in producing a uniform stock mixture in concentric thick stock dilution before the fan pump.

Concentric mixing before the fan pump, if not done properly, can significantly affect the spatial and temporal consistency and chemical uniformity of the stock leaving the approach flow area, leading to severe MD and CD nonuniformities in the final sheet. TAPPI recently published approach flow guidelines for concentric mixing used for thick stock dilution before the fan pump [1]. However, in view of the importance of thick stock dilution, it was considered that a rigorous analysis of concentric mixing was in order and the velocity ratio criteria reexamined.

When two fluid streams enter a concentric mixing region at different velocities, a high shear region forms at the interface between the two fluid streams. Instabilities at this interface cause vortex pairing, intertwining, and rollup. As the vortices evolve downstream, the annular stream cascades toward the center while the center jet disintegrates radially, enabling mixing. The degree of mixing can depend on the following [2]: the ratio of inner-to-outer pipe diameter, flow rate or velocity; the ratio of specific gravity between the two fluid streams; the inner and outer pipe Reynolds numbers; the pipe surface roughness; and any secondary pipe flows. When one of the constituents is a fiber suspension, additional parameters related to the fiber properties also affect the mixing process, which is further complicated by fiber flocculation [3-7].

The mixing of a relatively thick fiber stream with a dilute fiber stream or white water is common in the pulp and paper industry. Concentric mixing occurs both in chemical mixing and in the approach flow area immediately ahead of the fan pump, where thick stock (inner pipe) is diluted to the proper headbox consistency with clear accepts, secondary and tertiary screen accepts, deaeration overflow, etc. (outer annulus) [7]. When pulp and water streams mix concentrically, there is effective mixing when the shear stress provides enough energy to disrupt the fiber network between the two fluid streams. However, when the shear stress at the interface is less than the shear needed to disrupt the fiber network, the fiber network may not fracture and mix effectively. In concentric mixers, the shear stress can be managed by varying the flow rates of the streams.

In this study, the concentric mixing process is experimentally investigated using hardwood fiber stock and water streams. We compared experimental results with numerical predictions computed using the standard k-ε turbulence model.

EXPERIMENTAL EQUIPMENT AND SETUP

Concentric mixing involves mixing a "primary" fluid from an inner pipe with diameter d, volumetric flow rate q, and mean fluid velocity u, with a "secondary" fluid in an outer pipe of diameter D, volumetric flow rate Q, and mean fluid velocity v (**Fig. 1**). The primary fluid can have a specified species concentration C_p and the secondary fluid a species concentration C_s. One of the important operating parameters in the mixing process is the velocity ratio between the primary and secondary fluids ($R_v = u/v$).

The purpose of concentric mixing is to obtain a uniform species concentration within a short pipe distance from the jet nozzle. The jet issuing from the center pipe may be divided into two regions, the potential core region and the entrainment or mixing region (Fig. 1). The characteristics of the potential core are identical to those of the primary fluid stream while the characteristics of the mixing region vary from those of the primary fluid to those of the secondary fluid.

In this study, we evaluate the concentric mixing performance of a short fiber-water system. The primary fluid is a bleached hardwood pulp suspension (**Table I**) at one of three consistencies and is delivered to the mixing region through the center pipe. The secondary fluid is water.

Experimental Equipment

The experimental system consists of two transparent concentric pipes in the test section, a primary fluid mixing tank, a secondary fluid supply tank, a discharge tank, a pump, and associated piping, valves, and flow meters (**Fig. 2**). The test section consists of a transparent inner pipe with inside diameter d = 2.54 cm and a pipe wall thickness of 0.32 cm (**Fig. 3**) and a transparent outer pipe with inside pipe diameter D = 6.35 cm. The inner pipe protrudes into the outer pipe approximately ℓ = 39.4 cm after the 90^o bend (Fig. 3). The outer pipe extends approximately L = 58 cm beyond the inner pipe trailing edge before exiting into the discharge tank. Although L = 58 cm, the actual mixing region captured by high-speed video is approximately 25.4 cm downstream of the inner pipe trailing edge, corresponding to a mixing region of approximately 4D.

To measure the mixing efficiency (concentration profile), we introduced four sampling probes into the mixing pipe at a distance 3.9D downstream from the nozzle. The diameters of the sampling tubes are relatively large compared with the fiber size to avoid clogging, and the sampling tube walls are thin enough to minimize their effect on the flow field. The probes have outside diameters of 18 mm and wall thicknesses of 1 mm and are located at center and off-center of the main pipe (**Fig. 4**). We used high-speed video equipment (Olympus America Motion Analyzer with a frame rate of 1000 frames/sec) to qualitatively assess the mixing process.

Mixing Experiments

Approach. During the experiments, the mean secondary fluid (water) velocity was held constant at approximately v = 1.3 m/s, while the mean primary fluid (hardwood pulp) velocity was varied between 1.3 m/s to 7.76 m/s, corresponding to a mean velocity ratio range of $1 < R_v < 6$ (**Table II**). Pulp feed consistencies of 0.97%, 1.86%, and 2.91% were tested to address the effect of fiber concentration.

Experimental Analysis

We used probe samples to determine the concentration distribution in the concentric mixer. The uniformity (homogeneity) of the mixture was characterized by determining the second moment of fiber concentration (mixing) M for the pipe cross-sectional area. M $\left(=\sigma^2/\bar{c}^2\right)$ is the square of the variation coefficient and was previously defined by Gray [8] and Maruyama et al. [9] as,

$$M = \frac{1}{A}\int_A \left(\frac{c}{\bar{c}} - 1\right)^2 dA \,, \qquad (1)$$

where A is the cross-sectional area of the main pipe, D is the main pipe diameter, $\bar{c}$ is the mean fiber concentration in the mixer, and c denotes the local fiber concentration in a given sample probe. The mean fiber concentration $\bar{c}$ can be written as:

$$\bar{c} = \frac{q}{q+Q} c_o \,, \qquad (2)$$

where c_o, Q, and q represent the initial jet fiber concentration, the outer pipe volumetric flow rate, and the jet (inner pipe) flow rate, respectively. After computing the concentration distribution over the pipe cross section, M is approximated by the sum of the squares of the local fiber concentration difference from the mean value, written as follows:

$$M = \frac{\sum_{i=1}^{4}\left(\frac{c_i - \bar{c}}{\bar{c}}\right)^2 a_i}{\sum_{i=1}^{4} a_i} \,, \qquad (3)$$

where a_i and c_i are the area and pulp concentration of each sample, respectively. When the fluid is uniformly mixed, the second moment of mixing approaches zero. Hence, M characterizes mixing quality.

The mixing uniformity range U is defined as the normalized difference between the mean and local consistencies, as follows:

$$U = \frac{c - \bar{c}}{\bar{c}} \qquad (4)$$

This measure allows quantification of the change in the range of concentration distribution relative to the fiber mean concentration. It characterizes the mixing quality and the degree of difference of the concentration, compared with ideal streams where mixing would be complete and uniform.

By using longer sampling times, we obtained stable and consistent sampling data. The maximum relative uncertainty in U was 1.7%; most of the data were below 1%. For M the maximum relative uncertainty was 4.8%; most of the data were below 3.5%. The measured consistencies themselves generally had uncertainties less than 1%.

EXPERIMENTAL RESULTS

Figure 5 illustrates typical high-speed video stop-action images of the mixing experiments for the highest consistency (2.9%) evaluated. The bright region downstream of the inner pipe nozzle is the mixing region, which increases radially as the fluids move downstream. The outer pipe boundary is clearly identifiable, and the inner pipe can be recognized by its tip, captured on the left-hand side of the image. The total length of the mixing region captured by the images is approximately 4D downstream of the nozzle exit. The white region is the fiber stock, and the mixing process can be seen from the dispersion of the pulp that had been introduced in the center jet. The sampling ports at 3.9D are located near the right-most "+" mark (visible at the very right-hand side of each image in Fig. 5).

Effect of Velocity Ratio (R_v)

When the velocity ratio is near isokinetic ($R_v = 1$), there is a gradual radial increase in the jet directly downstream of the trailing edge of the inner pipe, even though the inner and outer jet mean velocities are nearly identical (Fig. 5a). This agrees with the flow character reported by Dahm et al. [10] for concentric mixers. Although the center jet wall thickness was very small in their case, they concluded that the boundary layer on both sides of the inner pipe introduced a wake. The evolution of the wake instability caused the two fluid streams to intertwine at the interface. In the current experimental geometry, boundary layers are present on both sides of the inner pipe, creating a velocity defect. The inner pipe has a finite thickness, resulting in wake formation.

Through inspection of multiple images of the $R_v = 0.9$ mixing process, large vortex rings and weave-like coherent structures are seen along the interface between the two fluids. These structures become unstable as the fluid moves downstream, with hydrodynamic instabilities and large-scale turbulent interactions that propagate downstream. This indicates that when the streams are near isokinetic, mixing results primarily from large-scale, low-intensity interactions.

As the mean velocity ratio increases, the mixing region changes from snakelike to a uniform cone-like shape (Figs. 5b and 5c versus 5a). The inner jet spread angle increases (the jet spreads faster), the large vortex rings observed in the isokinetic case are no longer apparent, and the mixing intensity and level of entrainment increase. Mixing is transformed from a large-scale, low intensity process to a small-scale, high-intensity process. In addition, the inner jet and downstream mixing regions appear more uniform. This is the result of the increase in center jet flow rate, which increases the local fiber concentration of the mixture (see Eq. 2) and the flow turbulence, augmenting the mixing. It is also the result of the large velocity difference between the inner and outer fluids, which creates the shear region and enhances small-scale turbulent mixing, creating a more uniform mixture. Similar trends were observed at the lower thick stock consistencies investigated.

The improvement in the mixing at higher velocity ratios is quantified using the second moment of mixing (M) and the mixing uniformity range (U) (**Tables III-V** and **Fig. 6**). As the mixture becomes more uniform, the difference between the samples and the mean mixture concentration approaches zero, as do M and U. The decreases in both M and U at higher R_v are consistent with the qualitative experimental observations discussed above.

Effect of Stock Consistency

For the three thick stock consistencies investigated, the weave-like structure at the center becomes unstable with increasing downstream distance from the nozzle. However, at higher consistency and low velocity ratio, the weave-like structure is stabilized by the fiber suspension and network formation, while mixing quality degrades—particularly when the velocities of the streams are approximately equal. This is indicated from the qualitative decrease in jet spread angle and the increase in M and U for the isokinetic data at higher consistency and low velocity ratio (Fig. 6 and **Fig. 7**, Tables III and IV). This is a result of the increase in fiber network strength with concentration, thus requiring more energy to disrupt the fiber network and mix with the water in the annulus.

The consistency effect is not apparent when the flow is in the turbulent range (stock mean velocity near or higher than the estimated fully developed turbulent velocity V_{turb}, discussed below). At R_v of approximately 3 and 6, there are no clear indications that increasing fiber consistency has a consistent and significant effect in hampering the mixing process (Tables III-V; Fig. 6). This seems to indicate that once the shear stress needed to fracture the fiber network is delivered, the fiber stock mixes in a similar manner regardless of the fiber consistency.

NUMERICAL MODEL

Governing Equations

The governing equations for conservation of mass, momentum, and concentration for steady, incompressible, turbulent viscous fluid flow with constant fluid properties are:

$$\frac{\partial u_i}{\partial x_i} = 0 \qquad (5)$$

$$\rho u_j \frac{\partial u_i}{\partial x_j} = -\frac{\partial p}{\partial x_i} + \frac{\partial}{\partial x_j}\left[(\mu + \mu_t)\left(\frac{\partial u_i}{\partial x_j} + \frac{\partial u_j}{\partial x_i}\right)\right] \qquad (6)$$

$$\rho u_j \frac{\partial c}{\partial x_j} = \frac{\partial}{\partial x_j}\left[\left(\frac{\mu}{Sc} + \frac{\mu_t}{\sigma_c}\right)\frac{\partial c}{\partial x_j}\right] \qquad (7)$$

All quantities have been time-averaged in the above equations, and u_i (i = 1, 2) are the mean local velocity components in the axial and radial directions. Also, ρ is the fluid density, p is the time-averaged pressure, μ is the dynamic viscosity, μ_t is the eddy (turbulent) viscosity, c is the time-averaged local fiber concentration, Sc is the Schmidt number, and σ_c is the turbulent Schmidt number (specified as $\sigma_c = 0.7$ in our calculations).

The governing equations are discretized and solved using FLUENT© computational fluid dynamics (CFD) software to simulate the mixing process as two turbulent miscible fluids with the same density and viscosity but different concentrations. FLUENT© uses a finite volume method to discretize the governing equations [11]. It was selected because it can be used to model the conservation equations of multiple fluid streams [12].

The eddy viscosity (μ_t) is specified through the standard k-ε turbulence model available in FLUENT© [12], allowing simulation of turbulent mixing. The standard k-ε model [13] is widely used because of its robustness, computational economy, and reasonable accuracy for a wide range of engineering problems. The basis of the model is that the eddy viscosity is defined by

$$\mu_t = \rho C_\mu \frac{k^2}{\varepsilon} \tag{8}$$

where C_μ is an empirical constant and k and ε are the turbulent kinetic energy and dissipation rates, respectively. These parameters are determined from the following transport equations

$$\rho u_j \frac{\partial k}{\partial x_j} = \frac{\partial}{\partial x_j}\left[\left(\mu + \frac{\mu_t}{\sigma_k}\right)\frac{\partial k}{\partial x_j}\right] + G_k - \rho\varepsilon \tag{9}$$

$$\rho u_j \frac{\partial \varepsilon}{\partial x_j} = \frac{\partial}{\partial x_j}\left[\left(\mu + \frac{\mu_t}{\sigma_\varepsilon}\right)\frac{\partial \varepsilon}{\partial x_j}\right] + C_{1\varepsilon}\frac{\varepsilon}{k}G_k - C_{2\varepsilon}\rho\frac{\varepsilon^2}{k} \tag{10}$$

where $C_{1\varepsilon}$ and $C_{2\varepsilon}$ are empirical constants, and σ_k and σ_ε are the turbulent Prandtl numbers for k and ε, respectively.

The G_k term represents the production of turbulent kinetic energy and is modeled by [12]

$$G_k = \mu_t S^2 \tag{11}$$

where S is the modulus of the mean rate-of-strain tensor defined by

$$S \equiv \sqrt{2S_{ij}S_{ij}} \tag{12}$$

with the mean strain rate given by

$$S_{ij} = \frac{1}{2}\left(\frac{\partial u_i}{\partial x_j} + \frac{\partial u_j}{\partial x_i}\right) \tag{13}$$

In the standard k-ε model, the following constant values are used as defaults in FLUENT©: C_μ = 0.09, $C_{1\varepsilon}$ = 1.44, $C_{2\varepsilon}$ = 1.92, σ_k = 1.0, and σ_ε = 1.3. Comments on the applicability of these values will be given below.

NUMERICAL RESULTS

The flow conditions are assumed to be axisymmetric to reduce the computational domain from three to two dimensions. The actual computation domain (**Fig. 8**) encompasses a radial distance of 3.175 cm (D/2) and an axial distance of 44.45 cm (7D) (1D length upstream of the trailing edge of the inner pipe and 6D length downstream). This region is discretized into a numerical computational grid of 36 x 300 nodes, with a slightly higher node density near the inner pipe trailing edge.

Because turbulence enhances the mixing process, the turbulence model used to simulate mixing plays a major role in determining realistic predictions. It has been shown that the values of the standard k-ε model constants, $C_{1\varepsilon}$ and $C_{2\varepsilon}$, affect the relative concentration of the mixing streams [14, 15]. Giorges and Heindel [16] showed that as $C_{2\varepsilon}$ increases, the length of the potential core of the inner jet decreases and the jet spread increases, and as $C_{1\varepsilon}$ increases, the potential core of the inner jet increases and the jet spread decreases. The latter trend is seen in **Fig. 9**, where change in $C_{1\varepsilon}$ from 1.7 to 1.88 results in a significant change in the numerically calculated concentration profile. For this study, we identified specific $C_{1\varepsilon}$ and $C_{2\varepsilon}$ values that provide reasonable qualitative agreement between the numerically predicted and experimentally observed concentration profiles.

We observe experimentally that when the velocity ratio is large, there is no clear indication that the mixing process is dependent on the concentration of the fiber suspension. However, for the isokinetic case, the mixing process is strongly affected by the concentration. Therefore, universal values of $C_{1\varepsilon}$ and $C_{2\varepsilon}$ are not appropriate for all cases. However, when the flow is turbulent and the velocity ratio is large, $C_{1\varepsilon} = 1.88$ and $C_{2\varepsilon.} = 2.4$ provide reasonable agreement with all experimental data that satisfy these two constraints.

Based on the Reynolds number alone, the streams are in the fully developed turbulent range. However, Reynolds number is not an appropriate measure of fiber suspension turbulence. A range of pulps and pipe diameters have been investigated to identify when fiber suspensions become turbulent [2, 17, 18]. Duffy [17] proposed Eq. 14 for the mean velocity V_w (m/s) at the onset of turbulence (also termed the onset of drag reduction) when the flow regime begins to transform from plug flow to transitional flow. (C is the oven-dried consistency in percent.) At this point, plug flow still exists, while a conventional Newtonian liquid (e.g., water) would already be in fully developed turbulence at the same bulk velocity [17]. Hemstrom et al. [19] suggested Eq. 15 for the mean velocity V_{turb} (m/s) for fully developed turbulent flow (onset of significant plug reduction) for an unbeaten, unbleached kraft pulp suspension:

$$V_w = 1.22\ C^{1.40} \tag{14}$$

$$V_{turb} = 1.8\ C^{1.4} \tag{15}$$

Using Eqs. 14 and 15, we calculated velocities where the pulp suspension is considered turbulent (**Table VI**).

Under conditions where the thick stock pulp is turbulent, we determined that a common set of constants, $C_{1\varepsilon} = 1.88$ and $C_{2\varepsilon.} = 2.4$, provide reasonable qualitative agreement of the experimentally observed concentration profiles with the numerical simulations. We reached this conclusion by comparing experimental and numerical concentration profiles at 3.9D for runs where the thick stock velocity exceeds the onset of drag reduction (comparing values in Table II versus Table VI) (**Figs. 10-12**). Under these conditions, we believe the shear stress at the interface is strong enough to overcome the fiber network strength. Thus, the two streams effectively mix as two miscible fluids. There are only small qualitative variations between the experimental and numerical results, with the largest variations near the mixer centerline (Figs. 10-12). (Differences between the experimental and numerical results cannot be fully explained by the uncertainties in the experimental consistency data, which, as mentioned above, were generally less than 1%.)

The dashed lines in Figs. 9-12 represent the numerical values for the local concentrations, while the symbols represent the averaged values (either numerical or experimental) over the specific probe areas (Fig. 4). For example, in Fig. 10 at r(m) = 0, the numerical results indicate a point mass fraction of 0.0164, while the average numerical value over $0 \le r(m) \le 0.009$ is 0.0143. The solid lines in Figs. 9-12 represent an approximation of the experimental concentration profiles, but are not regressed lines.

There is good qualitative agreement between the experimental and numerical results for those conditions that satisfy turbulent fiber suspension flow, as shown in **Fig. 13**. Similar results are found for other experimental conditions. From the experimental images, the white region at the center indicates the potential core and mixing region. The numerically simulated mixing process images show a darker region indicating the annular fluid (water) and a center, lighter region representing the center jet and mixing region between the two extremes. The interface of the two streams cannot be exactly predicted because of the time-averaged and steady state nature of the numerical results, but Fig. 13 gives a reasonable indication of the interface. However, the vortex ring that can be seen at the interface in the experimental image is not observed in the numerical simulations.

CONCLUSIONS

The experimental and numerical concentric mixing results reveal that increasing the velocity ratio increases the mixing effectiveness. In this case, the turbulence and the shear stress at the interface between the two fluid streams increase, causing the fiber network to break and mix with the water. Comparisons of the second moment of mixing, **M**, and the mixture uniformity range, U, for various velocity ratios, R_v, show that increasing R_v decreases **M** and U, demonstrating mixing process improvement. When the velocity ratio is high, the second moment of mixing is a stronger function of R_v than consistency (where no clear trend exists). That implies that once the shear stress disperses the fiber network, the flow behaves as if two turbulent Newtonian fluid streams are mixing. We believe this is why the numerical simulations are in close agreement with the experimental results when the thick stock velocity exceeds that required for turbulent fiber suspension flow. When the fiber stream is turbulent, the concentric mixing process can be simulated using the standard k-ε model with $C_{1\varepsilon} = 1.88$ and $C_{2\varepsilon} = 2.4$.

The results in Fig. 6 clearly indicate the importance of high velocity ratio in producing a uniform stock mixture in concentric thick stock dilution before the fan pump. Hence, industrial concentric mixing system design must allow for use of high velocity ratios in the concentric mixing area as one requirement for a uniform stock mixture. At low velocity ratios, mixing is inadequate, even after a significant downstream distance. **TJ**

ACKNOWLEDGMENTS

The authors acknowledge the funding and support of the Member Companies of the Institute of Paper Science and Technology. The authors also thank Adele Garner for her contributions to this work. The authors also acknowledge the use of FLUENT software from Fluent, Inc. in this study.

LITERATURE CITED

1. TAPPI TIP0404-54, Headbox Approach Piping Guidelines, 2000. Available online at <http://www.tappi.org/index.asp?rc=1&pid=6824&ch=8&ip=>.
2. Forney, L.J., "Jet Injection for Optimum Pipeline Mixing," *Encyclopedia of Fluid Mechanics Volume 2 - Dynamics of Single-Fluid Flows and Mixing*, N.P. Cheremisinoff, Ed., Gulf Publishing Company, Houston, pp. 660-690 (1986).
3. Duffy, G.G., and Lee, P.F.W., *APPITA J.* 31(4): 280(1978)
4. Stenuf, T.J., and Unbehend, J.E., "Hydrodynamics of Fiber Suspensions," *Encyclopedia of Fluid Mechanics: Vol. 5 - Slurry Flow Technology*, N.P. Cheremisinoff, Ed., Gulf Publishing Company, Houston, pp. 291-308 (1986).
5. Kerekes, R.J., and Schell, C.J., *J. Pulp Paper Sci.* 18(1): J32(1992).
6. Helmer, R.J.N., Covey, G.H., and Lai, L.C.-Y., *APPITA J.* 52(3): 197(1999).
7. Norman, B., and Tegengren, A., *Paper Tech.* 31(1): 42(1990).
8. Gray, J.B., "Turbulent Radial Mixing in Pipes," *Mixing: Theory and Practice*, Vol. III, Ch.13. Academic Press, 1986.

9. Maruyama, T., Mizushina, T., and Hayashiguchi, S., *Kagaku Kogaku Ronbunshu*, 8(4): 1(1982).

10. Dahm, W.N., Frieler, C.E., and Tryggvason, G., *J. Fluid Mech.* 241: 371(1992).

11. Patankar, S.V., *Numerical Heat Transfer and Fluid Flow*, Hemisphere Publishing Corp., New York, 1980.

12. Fluent Incorporated, "FLUENT 5 Users Guide," Lebanon, NH, Fluent, Inc., 1998.

13. Jones, W.P., and Launder, B.E., *Int. J. Heat Mass Trans.* 15: 310(1972).

14. Monclova, L.A., and Forney, L.J., *Ind. Eng.Chem.Res.* 34(4): 1488(1995).

15. Giorges, A.T., Forney, L.J., and Wang, X., "Numerical Study of Multi-Jet Mixing," *Transactions of the Institute of Chemical Engineers, Part A*, Vol. 79, pp. 515-522 (2001).

16. Giorges, A.T., and Heindel, T., "Concentric Mixing of Two Similar Fluids," AIChE 2000 Annual Meeting, November 12-17, 2000, Los Angeles, CA.

17. Duffy, G.G., "Flow of Medium Consistency Wood Pulp Fiber Suspensions," 47th APPITA Annual General Conference Proceedings, pp. 507-514 (1993).

18. Duffy, G.G., "How to Determine Pipe Friction Loss for the Design of Stock Piping Systems", *Proceedings TAPPI Engineering Conference*, pp. 247 (1979).

19. Hemstrom, G., Moller, K., and Norman, B., *TAPPI J.* 59(8): 115(1976).

Received: March 11, 2003
Accepted: January 28, 2004

INSIGHTS FROM THE AUTHORS

Why did you choose this topic to research? ***This project met an industry need, and it provided a challenging scientific problem.***

How does this research either complement and support previous research you (or others) have done, or how does it differ from previous research? ***This project links directly to the Fluid Dynamics/Forming research effort at IPST.***

What was the most difficult aspect of this research and how did you address that? ***The most difficult aspects of this research were the experimental work at the higher consistency levels, and the simulation work needed to agree with experimental results.***

What did you personally discover from this research? What was most interesting or surprising about your findings? ***We confirmed the importance of high velocity ratio, and how dramatically velocity ratio affects thick stock mixing. One very interesting finding was the ability to use the k-e model to simulate turbulent mixing.***

How might mills benefit from or use this information? ***Mills will benefit via improved design of the approach flow system to provide better mixed stock to the machine, improving MD uniformity.***

What's the next step? ***Followup work on softwood mixing will be presented at the TAPPI 2004 Spring Technical Conference, May 2004.***

White is with the Institute of Paper Science and Technology at Georgia Tech, Atlanta, Georgia 30332, Giorges is with Georgia Institute of Technology, Atlanta, GA 30332; Heindel is with Iowa State University, Ames, Iowa 50011. Email White at david.white@ipst.gatech.edu.

This paper is summarized in the May 2004 issues of *TAPPI JOURNAL* (Vol. 3: No. 5) and Solutions! For People, Processes and Paper magazine (Vol. 87: No. 5).

Table I. Hardwood pulp fiber length distribution, curl, kink, and percent fines. (Fiber Quality Analyzer, OpTest Equipment, Inc., Hawkesbury, Ontario, Canada).

	Sample 1	Sample 2
Mean length		
Arithmetic (mm)	0.48±0.010	0.468±0.010
Length weighted (mm)	0.739	0.730
Weight weighted (mm)	0.926	0.917
Mean curl index		
Arithmetic	0.053±0.002	0.054±0.002
Length weighted	0.056	0.058
Percent fines		
Arithmetic (%)	13.2	13.6
Length weighted (%)	1.98	2.09
Mean kink		
Kink index (1/mm)	1.09	1.09
Total kink angle (º)	17.0	17.3
Kinks per mm (1/mm)	0.63	0.65

Table II. Flow conditions used in the hardwood fiber stock-water concentric mixing experiments, with thick stock consistencies of 0.97, 1.86, and 2.91%.

Consistency	Stream	Volumetric Flow Rate (gal/min)	Volumetric Flow Rate (lit/min)	Mean Velocity (m/s)	Mean Velocity Ratio
0.97%	Primary	10.4	39.4	1.29	1.00
	Secondary	50.4	191	1.29	
	Primary	29.9	113	3.72	2.89
	Secondary	50.3	190	1.29	
	Primary	58.5	221	7.28	5.68
	Secondary	50.0	189	1.28	
1.86%	Primary	10.6	40.1	1.32	1.02
	Secondary	50.6	191	1.30	
	Primary	30.5	115	3.80	2.95
	Secondary	50.1	190	1.29	
	Primary	56.4	213	7.02	5.56
	Secondary	49.2	186	1.26	
2.91%	Primary	9.56	36.2	1.19	0.91
	Secondary	50.8	192	1.30	
	Primary	31.5	119	3.92	3.07
	Secondary	49.8	188	1.28	
	Primary	50.2	190	7.64	5.92
	Secondary	50.2	190	1.29	

Table III.Concentration distribution at 3.9D downstream for 0.97% hardwood fiber stock mixing.

Velocity ratio = 1.0 and mean consistency after mixing = 0.17%				
Sample #	Consistency (%)	Uniformity		
		$U=(c-\bar{c}) / \bar{c}$	U Range	M
1	0.091	-0.46	+1.17 to -0.46	0.19
2	0.118	-0.30		
3	0.369	1.17		
4	0.198	0.17		
Velocity ratio = 2.88 and mean consistency after mixing = 0.36%				
1	0.220	-0.39	+0.86 to -0.39	0.12
2	0.272	-0.25		
3	0.669	0.86		
4	0.483	0.24		
Velocity ratio = 5.69 and mean consistency after mixing = 0.53%				
1	0.441	-0.17	+0.29 to -0.17	0.017
2	0.473	-0.11		
3	0.684	0.29		
4	0.574	0.082		

Table IV. Concentration distribution at 3.9D downstream for 1.86% hardwood fiber stock mixing.

Velocity ratio = 1.01 and mean consistency after mixing = 0.32%				
Sample #	Consistency (%)	Uniformity		
		$U=(c-\bar{c})/\bar{c}$	U Range	M
1	0.148	-0.54	+2.59 to -0.54	0.61
2	0.194	-0.39		
3	1.148	2.59		
4	0.435	0.36		
Velocity ratio = 2.95 and mean consistency after mixing = 0.70% (Sample 2 was contaminated and not used)				
1	0.421	-0.40	+0.73 to -0.40	0.10
3	1.211	+0.73		
4	0.877	+0.25		
Velocity ratio = 5.57 and mean consistency after mixing = 0.99%				
1	0.819	-0.17	+0.32 to -0.17	0.022
2	0.851	-0.14		
3	1.310	+0.32		
4	0.996	+0.01		

Table V. Concentration distribution at 3.9D downstream for 2.91% hardwood fiber stock mixing. (Samples were not obtained at lower velocity ratios because of sampling probe plugging.)

Velocity ratio = 5.92 and mean consistency after mixing = 1.60%				
Sample #	Consistency (%)	Uniformity		
		$U=(c-\bar{c})/\bar{c}$	U Range	M
1	1.39	-0.13	+0.28 to -0.13	0.013
2	1.45	-0.09		
3	2.05	0.28		
4	1.68	0.05		

Table VI. The turbulent velocity required for pulp flow.

Consistency	$V_w = 1.22\ C^{1.40}$ (m/s)	$V_{turb} = 1.88\ C^{1.4}$ (m/s)
0.97%	1.2	1.7
1.86%	2.9	4.3
2.91%	5.4	8.0

FIGURES

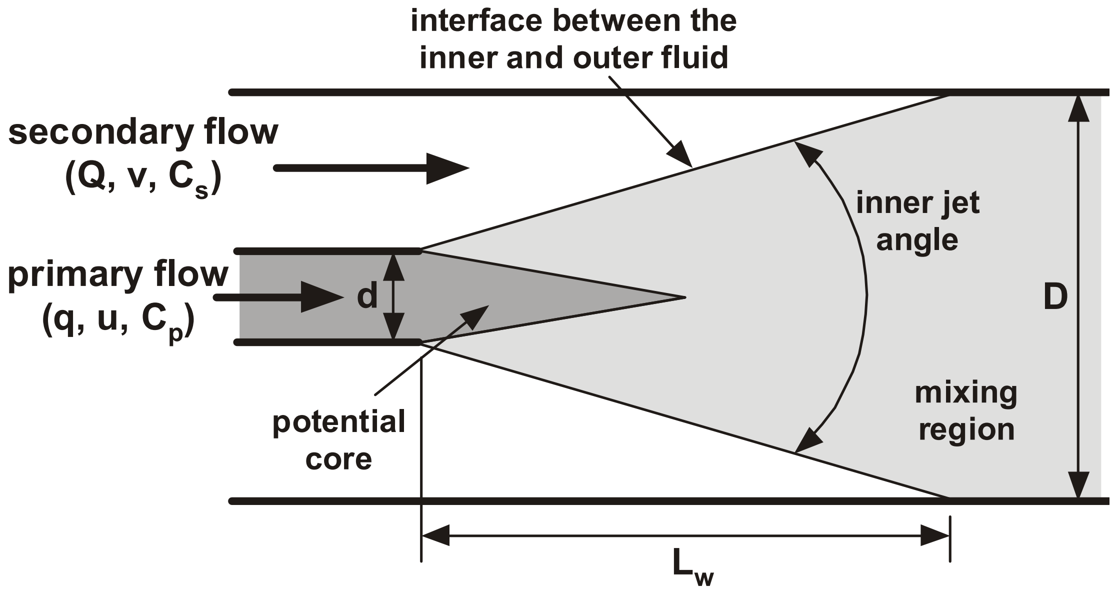

Figure 1: Schematic representation of the concentric mixing process.

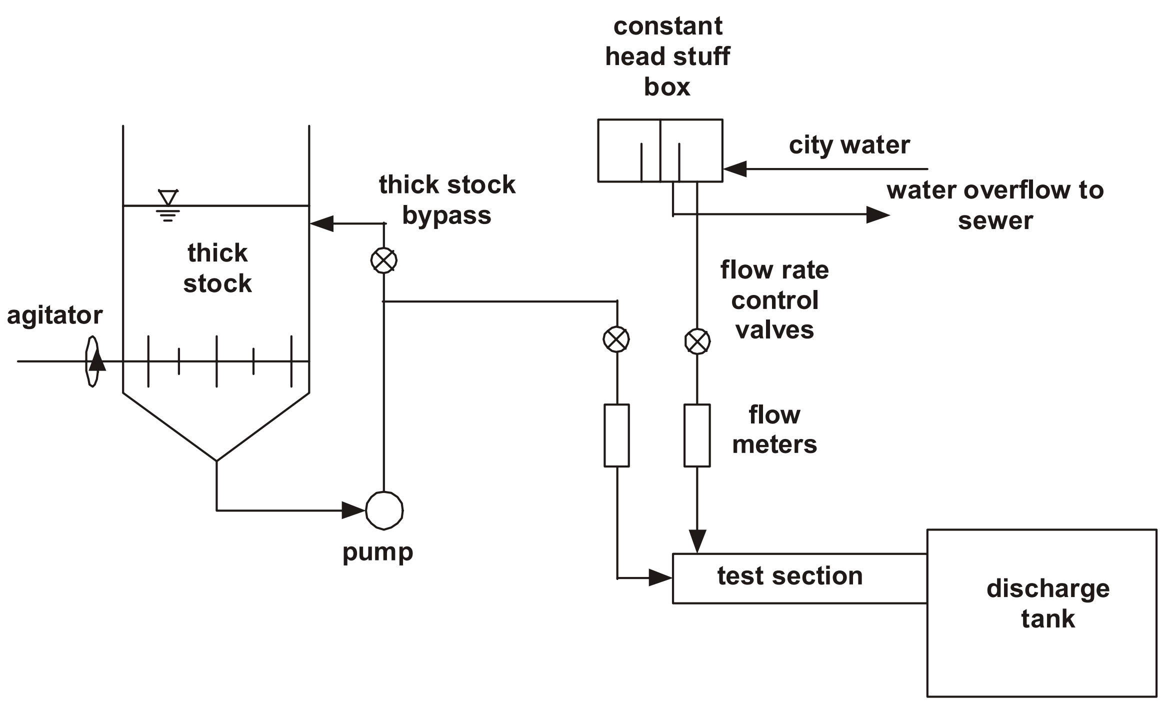

Figure 2: Experimental mixing facility.

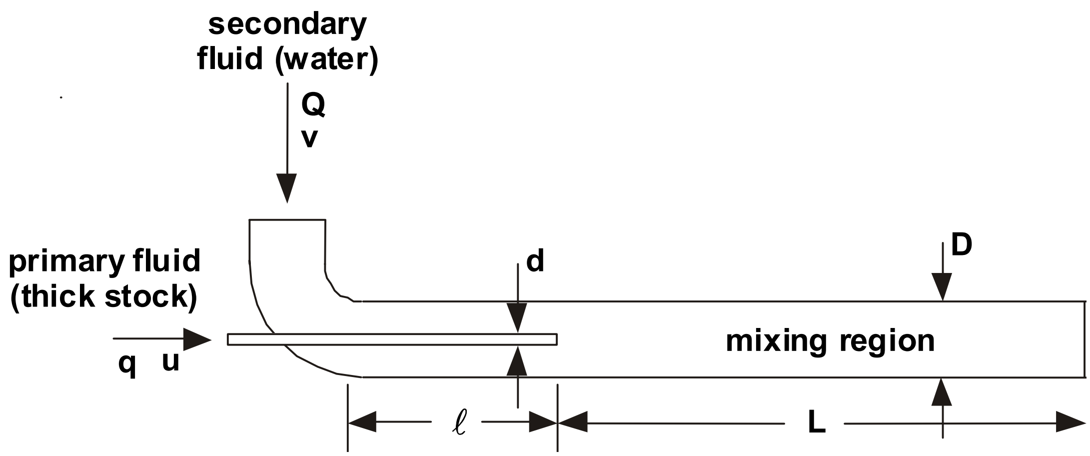

Figure 3: Concentric pipe mixer test section.

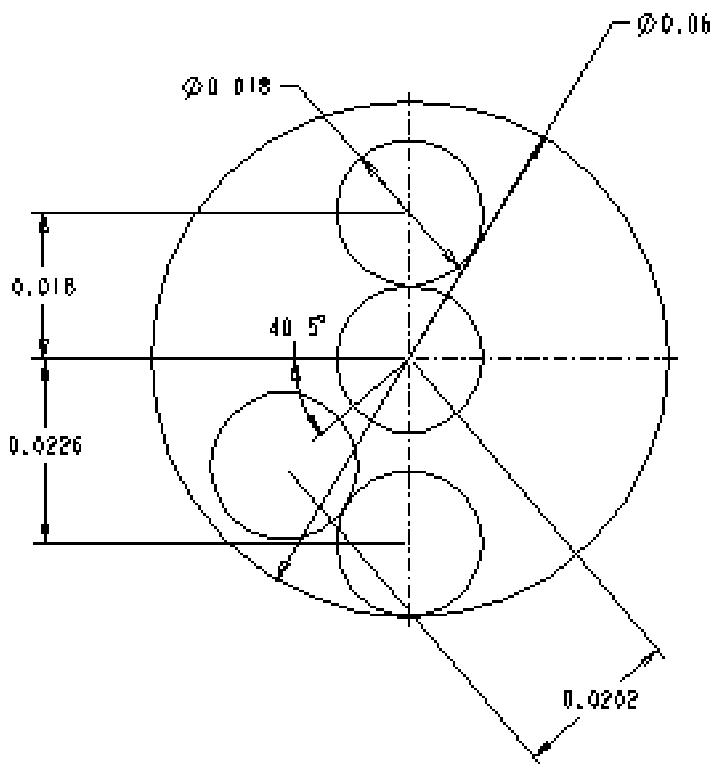

Figure 4: Sampling probes cross-sectional view. Units are meters.

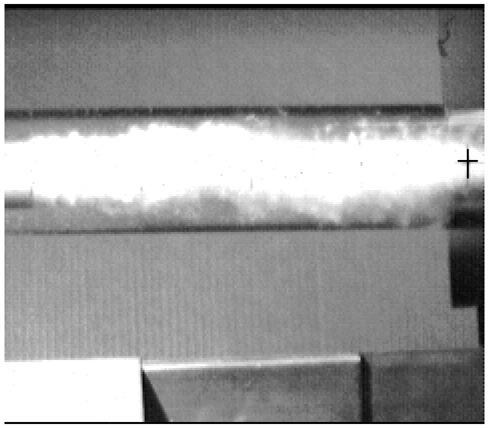

(a)

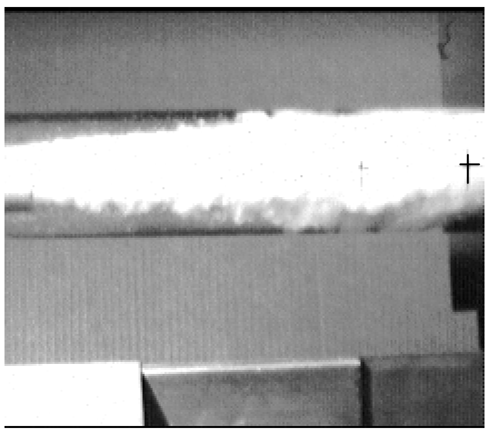

(b)

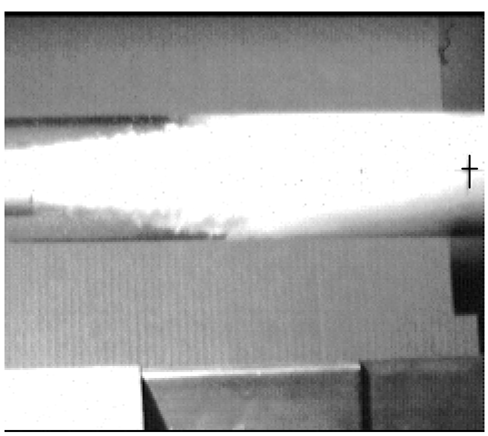

(c)

Figure 5: Images of 2.91% consistency hardwood fiber pulp and water mixing for various velocity ratios (R_v): (a) $R_v = 0.91$, (b) $R_v = 3.07$, and (c) $R_v = 5.92$. Flow is left to right.

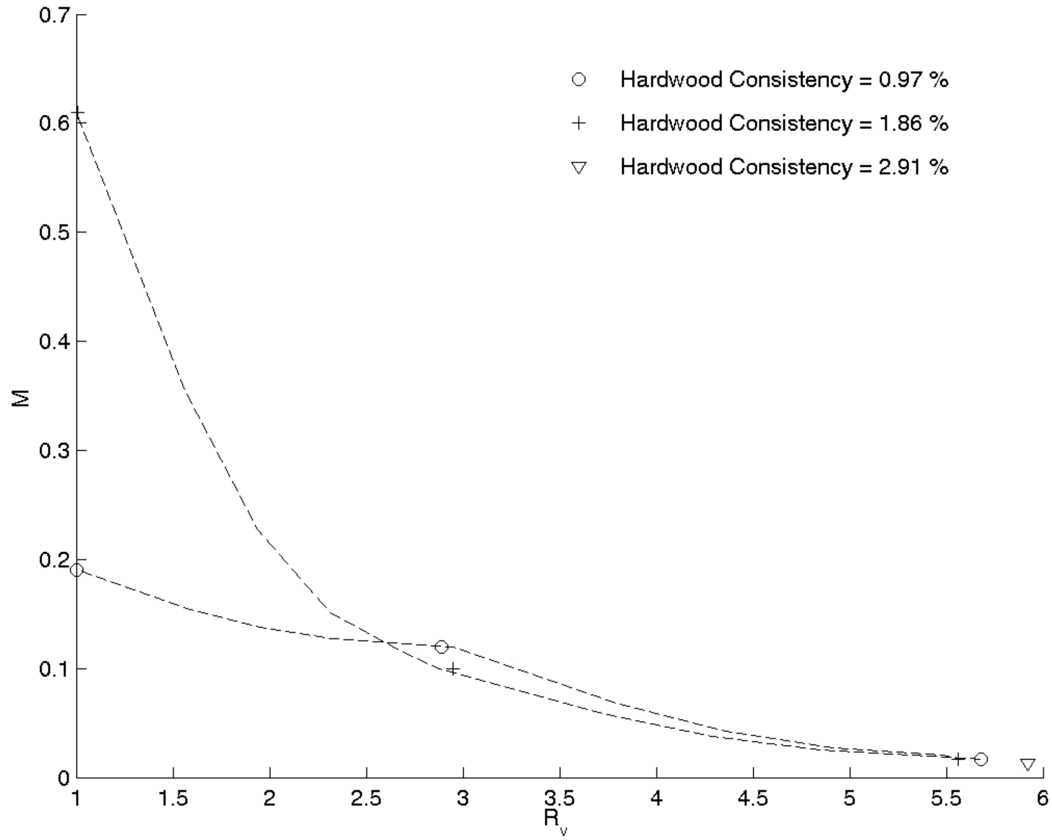

Figure 6: Second moment of mixing (M) vs. velocity ratio (R_v) for 0.97, 1.86, and 2.91% consistency hardwood pulp.

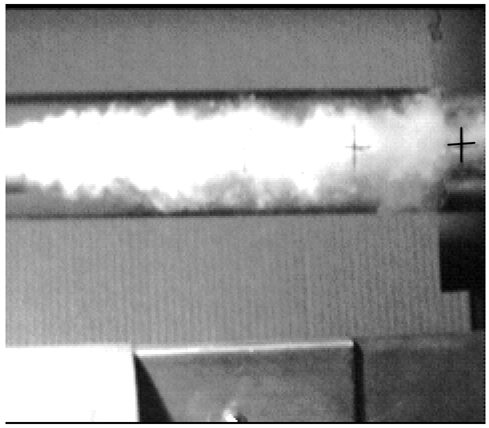

(a)

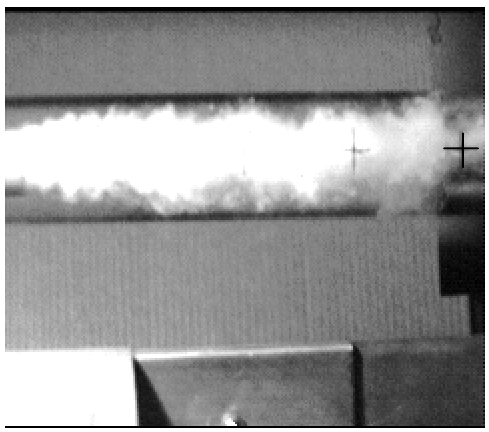

(b)

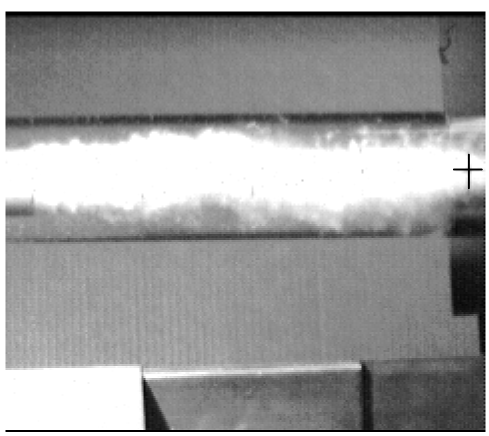

(c)

Figure 7: For R_v = 0.9-1.0, images of hardwood fiber pulp and water mixing at consistencies of (a) 0.97%, (b) 1.86%, and (c) 2.91%

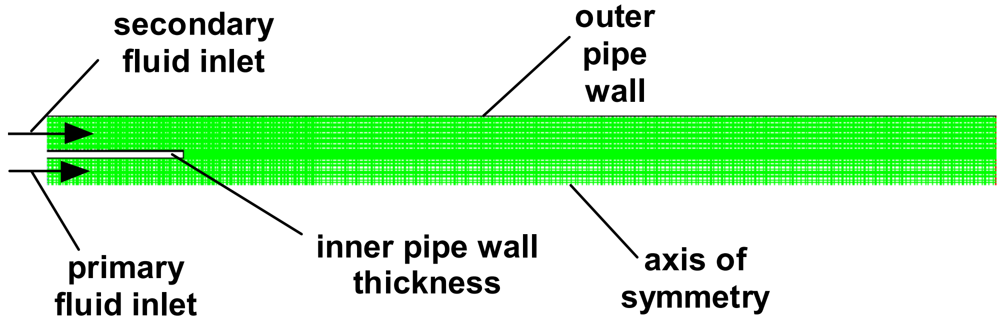

Figure 8: The axisymmetric computation domain.

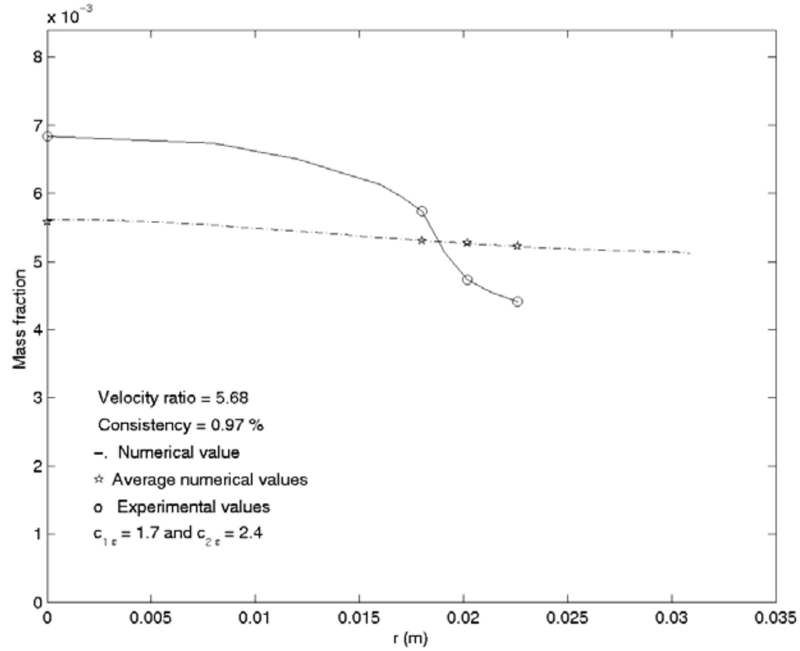

(a)

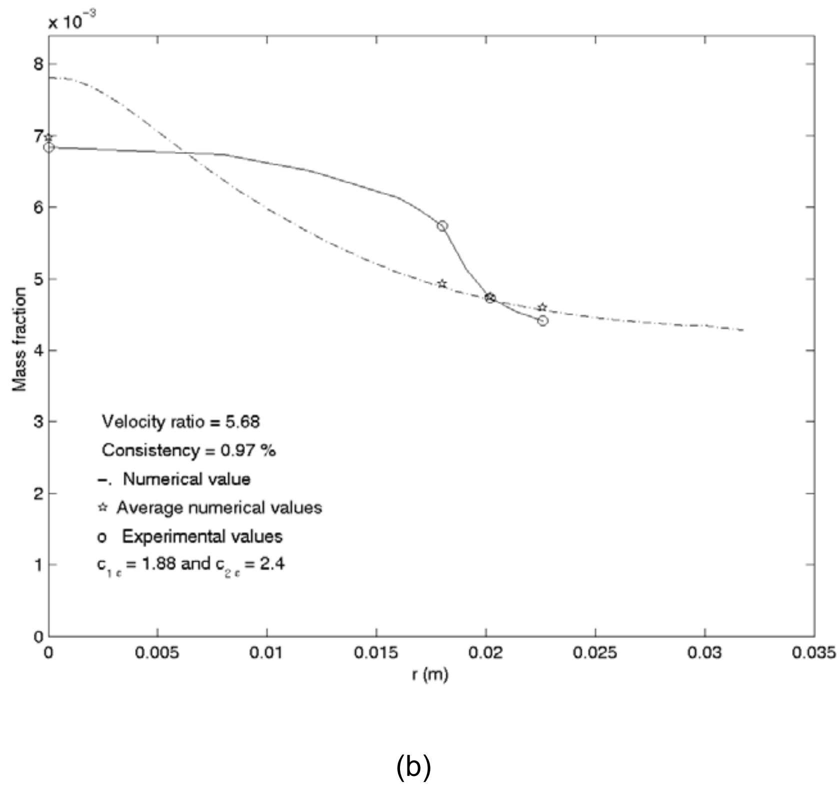

(b)

Figure 9: Experimental and numerical concentric mixing concentration profiles at 3.9D downstream for R_v = 5.68 and 0.97% thick stock consistency, standard k-ε model with (a) $C_{1\varepsilon}$ =1.7 and $C_{2\varepsilon}$ = 2.4 and (b) $C_{1\varepsilon}$ =1.88 and $C_{2\varepsilon}$ = 2.4.

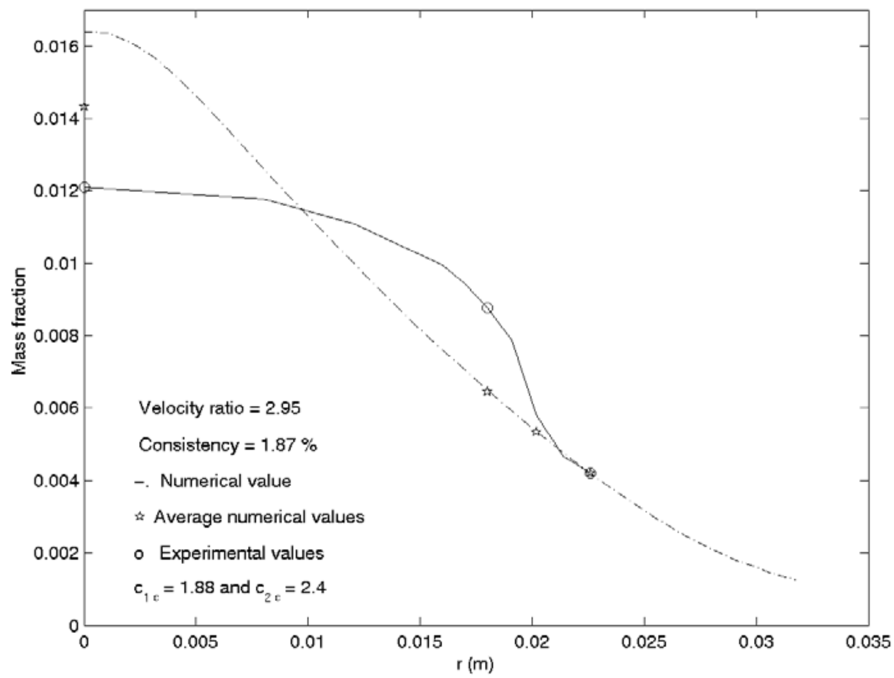

Figure 10: Concentric mixing concentration profile at 3.9D predictions for R_v = 2.95 and 1.86% consistency by the standard k-ε model for $C_{1\varepsilon}$ = 1.88 and $C_{2\varepsilon}$ = 2.4.

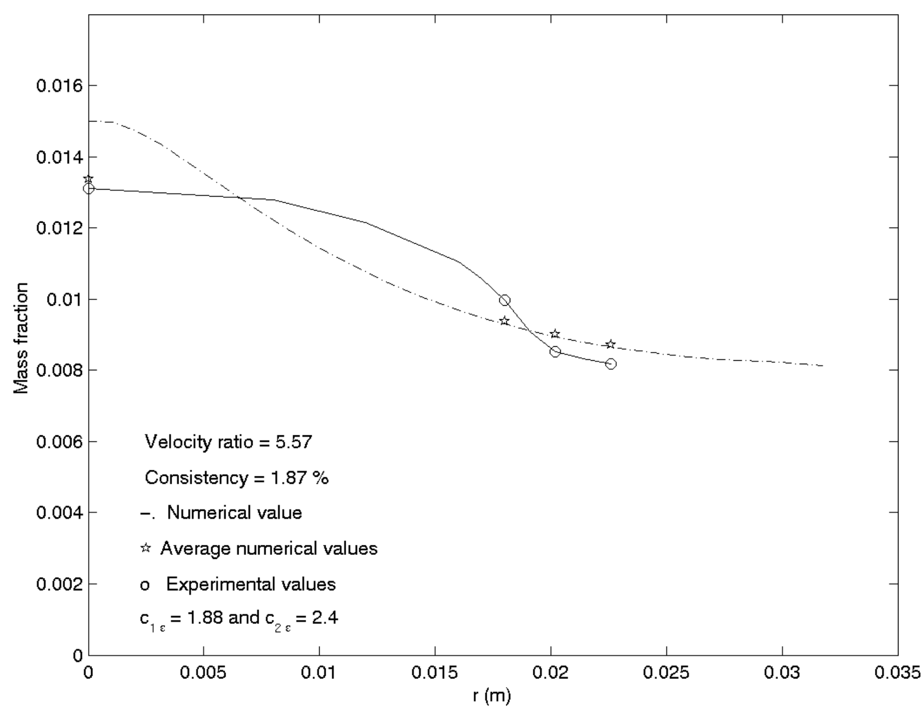

Figure 11: Concentric mixing concentration profile at 3.9D predictions for R_v = 5.57and 1.86% consistency by the standard k-ε model for $C_{1\varepsilon}$ = 1.88 and $C_{2\varepsilon}$ = 2.4.

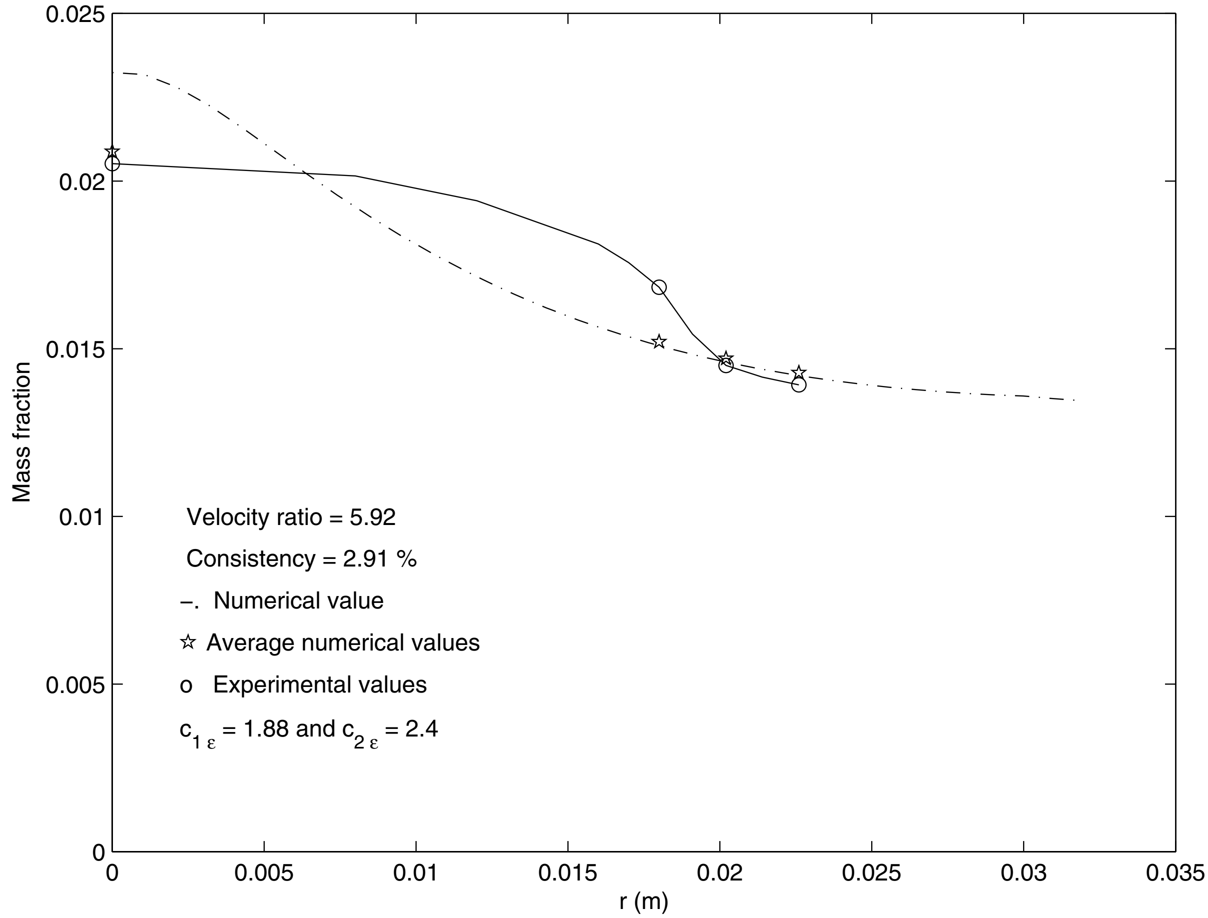

Figure 12: Concentric mixing concentration profile at 3.9D predictions for R_v = 5.92 and 2.91% consistency by the standard k-ε model for $C_{1\varepsilon}$ = 1.88 and $C_{2\varepsilon}$ = 2.4.

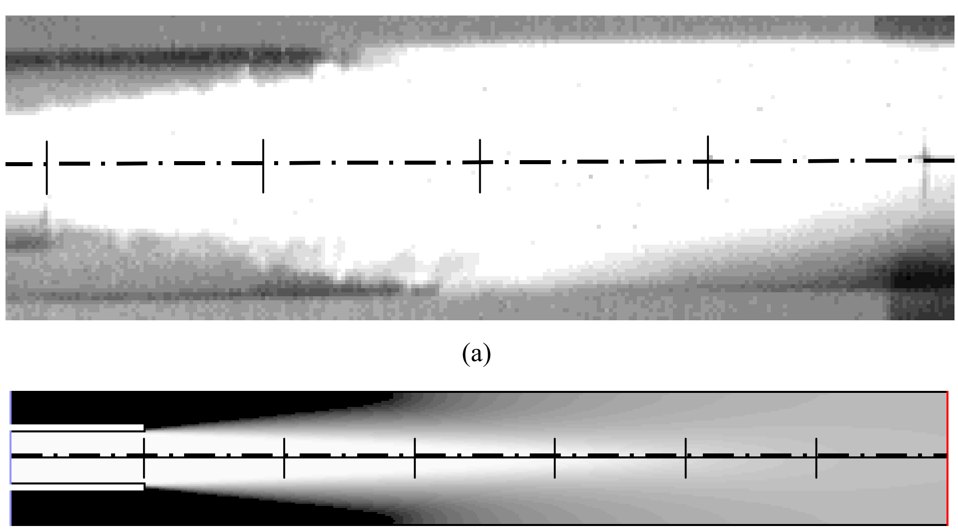

(a)

(b)

Figure 13: Comparisons between the experimental and predicted mixing regions for R_v = 5.92 and c = 2.91%: (a) Representative experimental image and (b) standard k-ε model predictions.